JOURNAL OF AIRCRAFT
Vol. 29, No. 5, Sept.–Oct. 1992

Experimental Study of Noise Generation and Propagation in a Turbofan Model

S. Lévy* and S. Canard-Caruana†
Office National d'Etudes et de Recherches Aérospatiales (ONERA), 92322 Châtillon, France
and
J. Julliard‡
Société Nationale d'Etude et de Construction de Moteurs d'Aviation (SNECMA), 77550 Moissy Cramayel, France

Acoustic radiation from subsonic fans is mainly due to blade- and vane-pressure fluctuations. Its prediction needs experimental data because computational aerodynamic models still do not accurately predict the high-order loading harmonics, that constitute the noise sources. The CA5 model fan with ONERA thin-film pressure transducers bonded on certain blades and vanes was tested in the SNECMA 5C2 compressor anechoic facility. Results are obtained on the influence of a hemispherical inflow-control device used to simulate flight effects in static tests. It is shown that the device reduces blade-pressure fluctuations as expected by about 10 dB in the low- and medium-frequency range (rotational harmonics from 1 to about 30). This explains the lower level of front-radiated noise at the blade-passing frequency observed in flight. The second step of the study is the modal analysis of the sound field in the inlet duct, with an application to the insertion loss produced by acoustic linings on the inlet duct wall. By isolating the rotor-stator interaction modes, it is found that a lining optimized for the blade-passage frequency (BPF) could produce a noise reduction in flight of 10 dB more than a broadband lining at the BPF.

Nomenclature

B = number of rotor blades
f = frequency
I = cross spectrum
j = order of a blade loading harmonic, $f = jN$
L = pressure level
L_{Coh} = coherent tone level
L_{Tot} = total tone level
m = spinning mode order
m_c = cut-off mode
m_I = rotor/stator interaction mode
N = fan rotation speed, N_0: design value
n = order of a blade-passage frequency harmonic, $f_n = nBN$
S = Fourier component of s
s = acoustic signal
T = fan rotation period, $T = 1/N$
t = time
V = number of outlet guide vanes
Γ = squared amplitude of S
ΔX = length of the fan throttle
θ = angle in a duct cross section
ν = radial mode order

Subscripts
F = fixed microphone
M = moving microphone

Introduction

IT is well established that front-radiated turbofan engine noise is mainly due to the tones radiated by the duct. The main sources of a subsonic fan are related to the blade and vane pressure fluctuations.[1] Contrary to propellers and open rotors, the mean load does not radiate noise because the duct introduces some cutoff properties on the generated spinning modes. At typical blade-passing frequencies, only the simplest space structures (acoustic modes) can propagate and radiate in the free field. These waves are due to high-order loading harmonics.

Theoretical models to predict the propagation and radiation of acoustic modes are well validated by experiments.[2,3] Aerodynamic computations are, however, still insufficient to calculate the fan loads up to high frequencies.[4] The prediction of acoustic level and far-field directivity thus requires accurate measurements of the noise sources and generated spinning modes.

Several laboratories have studied blade- and vane-pressure fluctuations, with the aim of improving the description of the noise sources. Reference can be made to the pioneer work of Heller and Widnall,[5] and to the numerous tests by Hanson.[6,7] It has also been recognized for a very long time that measurement of acoustic modes is essential in studies of fan or compressor noise.[8–10]

This article presents some new experimental studies performed in the SNECMA compressor anechoic test bench. They have been initiated by research programs on fans that are lighter and more compact than those of the present quiet turbofans, i.e., with fewer outlet guide vanes (OGV) and smaller rotor-OGV spacings. These projects need further progress in acoustics in order to maintain low sound levels. A major effort must be put on accurate flight simulation in static facilities and on optimization of duct acoustic linings.

After a brief description of the test rig and of the model fan under study, two main topics are discussed: 1) measurements of blade- and vane-pressure fluctuations by thin-film transducers, applied to the characterization of noise sources in simulated flight conditions with an inflow control device; and 2) spinning mode analysis of the sound field propagating in the intake, with emphasis on the insertion loss due to acoustic linings on the duct wall.

I. Test Facility

The tests are performed in the 5C2 compressor anechoic bench, at the SNECMA-Villaroche Center (Fig. 1). This fa-

Received Oct. 1, 1990; presented as Paper 90-3950 at the AIAA 13th Aeroacoustics Conference, Tallahassee, FL, Oct. 22–24, 1990; revision received Nov. 19, 1991; accepted for publication Nov. 22, 1991.

*Deputy Head of Acoustics Division, Physics Department, BP72. Member AIAA.
†Research Scientist, Physics Department, BP72.
‡Acoustics Research Manager, Technical Department.

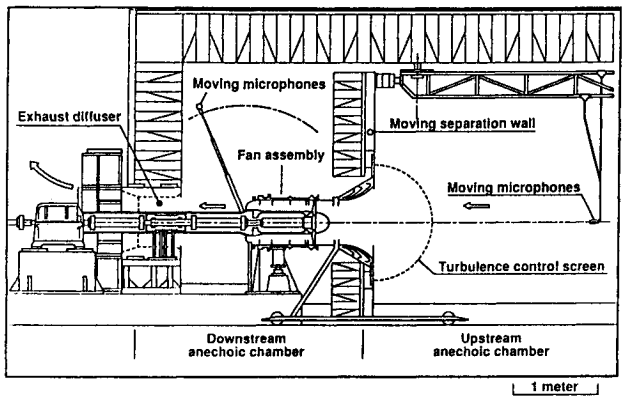

Fig. 1 SNECMA 5C2 compressor anechoic test facility.

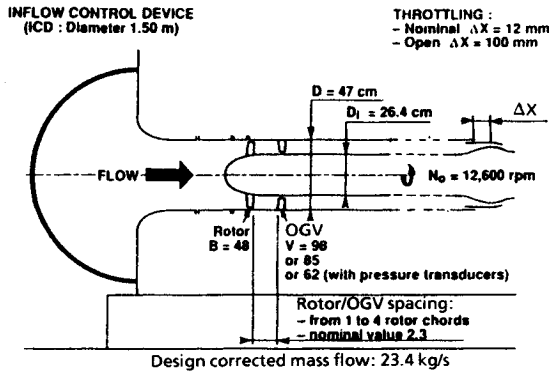

Fig. 2 CA5 model fan design features.

cility includes an upstream and a downstream anechoic room, with fixed and moving microphones measuring the directivity of the radiated noise.

The fan model under study here is a subsonic one, called CA5 (Fig. 2). The design rotation speed is N_0 = 12,600 rpm. Of the three stators used, only the one with V = 98 vanes satisfies the criterion $V > 2B$ of quiet engines, i.e., the rotor-stator interaction modes are cut off at the blade-passage frequency (BPF).[2,11] The interaction modes are also cut off at BPF with the 85-vane stator except at high speed, because V is close to $2B$. The 62-vane stator is used to test duct linings optimized to absorb the propagative interaction mode at BPF (see Sect. III). The axial rotor-OGV spacing is adjustable from 1 to 4 times the axial projection of the rotor chord, with a design value of 2.3. The throttle is settled by the axial adjustment ΔX of the downstream exit nozzle. All the results selected in this paper are obtained at the design throttle ΔX = 12 mm, unless otherwise specified.

It is also seen in Fig. 2 that the intake can be fitted with an inflow control device (ICD) in order to simulate the flight aerodynamic conditions.[11] As described in Ref. 12, it is of hemispherical shape with a diameter of approximately three times the inlet duct, and it principally incorporates a honeycomb and a wire-mesh on the internal side. The tests presented here are generally performed with the ICD, unless otherwise specified in the figure captions.

II. Measurements of Blade- and Vane-Pressure Fluctuations

A. Thin-Film Pressure Transducers

Since a model fan has very thin airfoils and high centrifugal accelerations, any machining of the blades would dramatically reduce the structural strength of the airfoils. For this reason, ONERA has developed its own thin-film pressure transducers, of the capacitive type, using metallized dielectric layers (polyimide films).[13] Since their overall thickness is less than 50 μm, they can be directly bonded to the profiles without disturbing the surrounding flow. The dielectric of the sensitive area (about 3 mm along the chord × 5 mm along the span) is punched with some 50 air-filled cavities. Pressure fluctuations produce the motion of the film over these cavities, and then capacity changes. The sensitivity is about 20 μV/Pa at a voltage of 100 V, with a flat response up to at least 100 kHz. The effects of the secondary parameters (acceleration, strain, temperature, and humidity) are negligible compared with that of the pressure fluctuations.

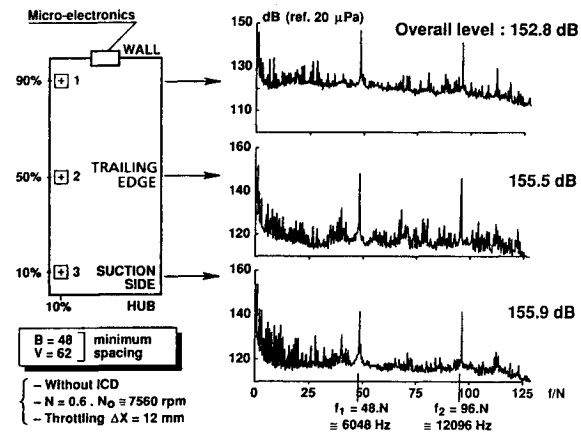

Fig. 3 Mean spectra of pressure fluctuations on an outlet guide vane.

Several tests were run with eight transducers distributed on three rotor blades. Blade-pressure signals are transmitted through a slip-ring after amplification. Only the 62-vane stator was instrumented and some tests were performed with six transducers distributed on two OGV. The exact locations of the transducers will be shown by inserts in the figures providing the experimental results.

B. Data Reduction

A one-per-revolution trigger is used to simultaneously digitize the signals from all the transducers at 256 N (N is the rotation speed in Hz). They are separated into blocks of 1024 data points, i.e., of duration of $4/N = 4\ T$, where T is the period of rotation. 100 consecutive samples are processed in order to obtain the ensemble-averaged waveform (in Pa vs time).

The mean spectrum is deduced from the averaged 100 fast-Fourier transforms (FFT). The spectrum of the enhanced time signature is also computed; it is the coherent spectrum since all the phenomena that are not synchronized with the rotation speed are eliminated (more precisely, they are reduced by $\sqrt{100}$, or 20 dB). The horizontal axes of both kinds of spectra are graduated in reduced frequency f/N. The maximum frequency is 128 N (an antialiasing filter slightly below this value is included before digitization), and the resolution is $N/4$. The vertical axes are graduated in decibels, with the same reference as in acoustics (20 μPa). The overall level is also calculated for each spectrum.

C. Outlet Guide Vane-Pressure Fluctuations

The investigation is limited to the leading-edge transducers on the OGV since it was established that the major contribution to the unsteady stator lift occurs near this location.[14] Figure 3 shows some spectra obtained at $N = 0.6\ N_0$ with three transducers on the suction side. The three spectra are very similar. If all blades and their wakes were identical, all pressure fluctuations would be at the blade-passage frequency $f_1 = BN$, and its harmonics. The rotational harmonics, that are much lower, are due to the differences from wake-to-wake.

In Fig. 4, the overall level, and the levels at BPF and at 2 BPF measured by transducer No. 1, are plotted as a function

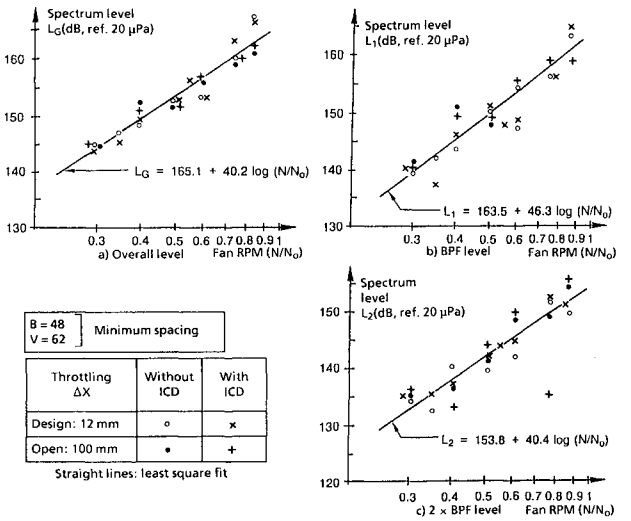

Fig. 4 Outlet-guide-vane leading-edge pressure fluctuations vs the rotation speed (logarithmic scale): Transducer No. 1 (see Fig. 3).

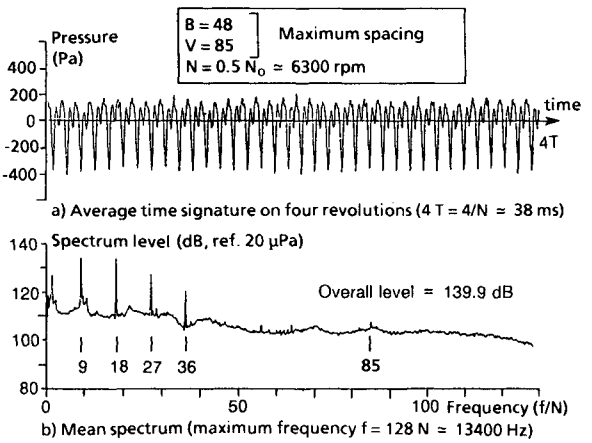

Fig. 5 Fan blade-pressure fluctuations (suction side, 0.8 span, mid-chord) due to an upstream ring of nine rods (8 mm diam).

of the rotational speed. Four series of tests are plotted together: at design and at open throttle, and both with and without the inflow control device. It clearly appears that the scatter of the levels is rather low and there is no definite difference between the four series of runs. Since the ICD greatly reduces the front-radiated noise at BPF, this result shows that the acoustic sources are mainly located on the first row, i.e., on the rotor in the present fan. Another feature of the figure is that the regression lines providing the least square fit through the experimental data approximately follow a law in 40 log (N/N_0), that confirms that the aerodynamic pressure fluctuations vary as the square of the velocity (the axial velocity and rotational speed remain nearly proportional).

D. Pressure Fluctuations Measured by a Blade Transducer

The following results are obtained in the configuration with the 85-vane stator at maximum rotor-OGV spacing. The selected blade-pressure transducer is located on the suction side at 0.8 span and approximately at midchord. The measurements on blades are less straightforward than those on vanes. In order to assess their validity, special tests were made with a ring of 9 radial rods 8 mm diam, located every 40 deg, 140 mm upstream of the blade leading edge. The results of a typical run are given in Fig. 5. The enhanced time signature, displayed in Fig. 5a, clearly shows the 4 × 9 wakes shed from the rods in four revolutions. As a consequence, the mean spectrum in Fig. 5b is dominated by the harmonics of 9N.

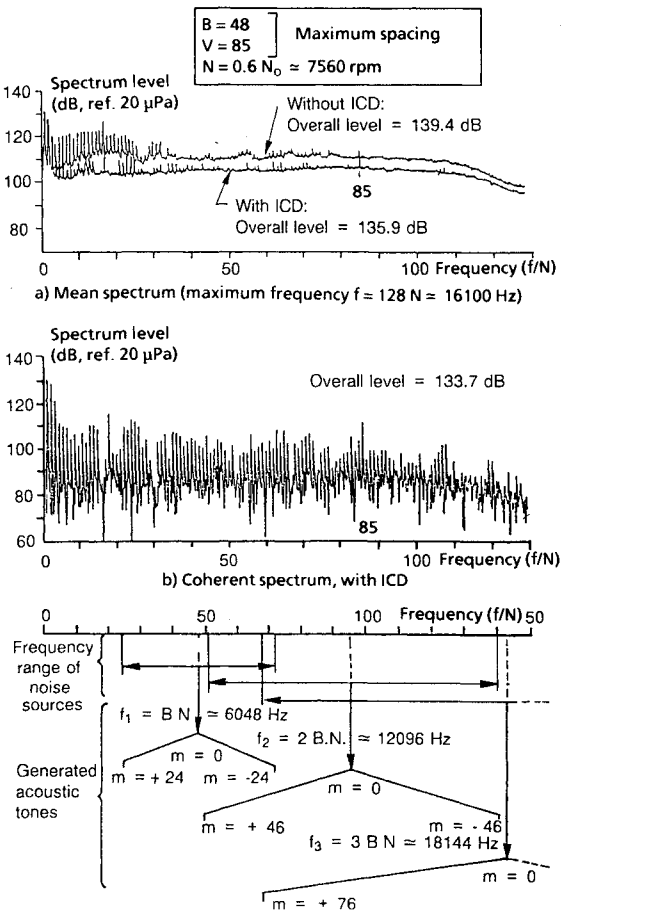

Fig. 6 Effect of an inflow control device (ICD) on blade-pressure fluctuations (suction side, 0.8 span, mid-chord).

A run in the basic configuration (without rods) is displayed in Fig. 6. Figure 6a superimposes the blade pressure spectra with and without the inflow control device. Many rotational harmonics appear in these mean spectra (they are not seen in Figure 5b because the wakes shed from the rods increase the broadband component). The rotational harmonics are mainly due to inflow disturbances lasting several cycles. It can be seen that the ICD reduces their level by about 10 dB up to the harmonic $j = f/N \simeq 30$, or $f \simeq 3.8$ kHz, i.e., a time scale greater than 0.3 ms or a length scale greater than 2 cm (based on a flow Mach number of 0.2 in the intake duct). This is actually the expected effect of the ICD, breaking the large vortices (the ground vortex for instance). The broadband turbulence is also reduced by about 5 dB even at higher frequencies. The overall level is only decreased by 3.5 dB because the first two intense lines at $f = N$ and $2N$ are higher with the ICD in this example. They are theoretically associated with the mean flow distortion on 360 deg, but a response to vibrations may disturb the measured signals at these frequencies.

The rotational harmonics are greatly reduced by the ICD, but they are not completely cancelled, as is shown by the coherent spectrum in Fig. 6b. It is also seen in Figs. 5 and 6 that the line $f = VN = 85N$ always emerges, although the rotor-OGV spacing is a maximum in both cases. This means that the interaction between the rotor and the potential field of the stator remains a non-negligible noise source.

All the rotational harmonics do not generate tone noise radiating into the free field because of the duct cutoff properties. The range of loading harmonics $f_j = jN$ generating propagative acoustic spinning modes $m = nB - j$ at $f_n = nBN$, is deduced from the Tyler and Sofrin model.[2] The cuton modes

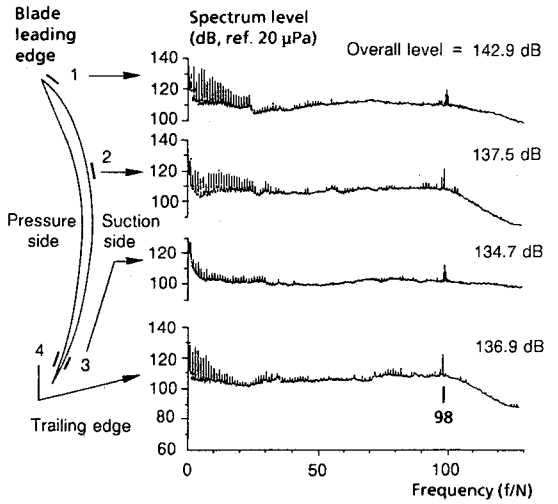

Fig. 7 Mean spectra of blade-pressure fluctuations at 0.8 span: B = 48, V = 98, design spacing, without ICD; N = 0.6, $N_0 \simeq$ 7560 rpm (maximum frequency f = 128, $N \simeq$ 16,100 Hz).

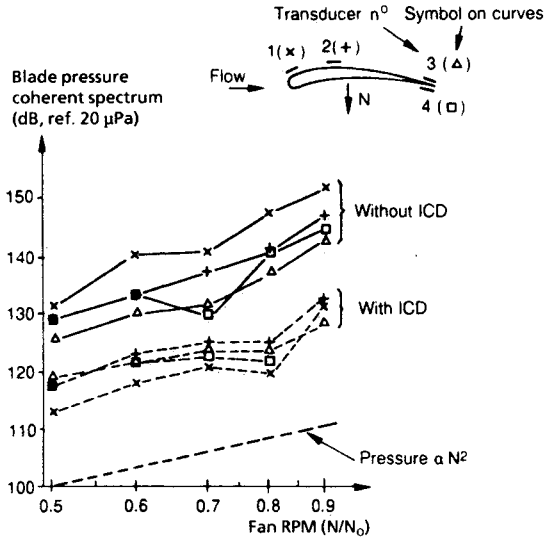

Fig. 8 Coherent overall level of blade pressure fluctuations vs the rotation speed (logarithmic scale): B = 48, V = 98, design spacing.

in the test conditions of Figs. 6a and 6b ($N = 0.6\ N_0$) are

$$|m| \leq 24 \quad \text{for} \quad f_1 = \text{BN}$$
$$|m| \leq 46 \quad \text{for} \quad f_2 = 2\text{BN}$$
$$|m| \leq 76 \quad \text{for} \quad f_3 = 3\text{BN}$$

As a consequence

$$24 \leq j \leq 72 \quad \text{for} \quad f_1$$
$$50 \leq j \leq 142 \quad \text{for} \quad f_2$$
$$68 \leq j \leq 220 \quad \text{for} \quad f_3$$

This is shown graphically in Fig. 6c. The horizontal scale is graduated in blade-loading harmonics $j = f/N$. The range of loading harmonics generating each acoustic frequency is marked out. It is seen e.g., that the stator field ($j = V = 85$) generates noise only on harmonics of the BPF but not on the BPF itself (see the more general comment in Sect. I). It is also found that the first cuton mode at $N = 0.6\ N_0$ is due to the harmonic $f = 24\ N \simeq 3$ kHz. This result emphasizes the interest of blade-pressure measurements (see the Introduction) because the study of noise sources requires the knowledge of high-order loading harmonics.

E. Pressure Fluctuations Along a Blade Chord

The study has been limited to only one transducer in the previous section. It needs to be supplemented at other blade locations. This is illustrated by tests with the 98-vane stator at design rotor-OGV spacing. The mean spectra along a blade chord at 0.8 span, without ICD, are given in Fig. 7, for $N = 0.6\ N_0$ (transducer No. 2 was the one selected in the above section). The pressure fluctuation due to the stator potential field ($f = 98\ N$) is higher than in Figs. 5 and 6 because the rotor-OGV spacing is smaller (design value). The three measurements along the suction side show that the overall level and the rotational harmonics decrease from the leading edge to the trailing edge, this confirms the hypothesis that they are due to upstream disturbances.

Figure 8 is a comparison of the blade-pressure fluctuations with and without ICD for the four transducers vs the rotational speed. The overall coherent level is plotted here in order to emphasize the effect of the ICD on tone noise. The curves approximately follow a pressure law in N^2 (as in Fig. 4). A decrease on the order of 10 dB is found with the ICD. This is in very close agreement with a similar study by NASA on a JT15D turbofan engine, with the aim of comparing static, wind tunnel, and flight tests.[15,16] Figure 8 also shows that the differences in the overall fluctuating pressure levels from leading edge to trailing edge on the suction side are greatly reduced with the ICD. Moreover, the leading-edge levels become lowest with the ICD (the attenuation due to the ICD reaches 20 dB for transducer No. 1). This certainly means that the measured signals are sensitive to the blade boundary-layer pressure fluctuations, that are lower than the inflow distortions without ICD.

III. Spinning-Mode Analysis of the Sound Field Propagating in the Intake Duct

It has been shown that the blade-pressure transducers provide unique measurements of the actual role of an inflow control device in a static bench. However, the blade-pressure spectrum is not the only parameter governing noise radiation, because only some of the loading harmonics generate propagating waves at a given acoustic frequency f (see Fig. 6c). A spinning mode is defined by f, and by the angular wave number m and the radial mode ν (m and ν are integers).

Measurement of acoustic modes is essential for several reasons:

1) High values of m cannot propagate in the duct, and thus do not radiate outside.

2) The directivity pattern in the free field strongly depends on the cuton ratio, i.e., the ratio between the cutoff frequency of the mode (m, ν) and the frequency f.

3) The space structure defines the angle of incidence of a spinning wave on the duct wall, and is an important parameter for designing optimized linings.

A. Data Processing

The method is based on the same principles as in Refs. 17 and 18. It is described in detail in Ref. 19. Two microphones are needed for determining the angular wave-number spectra. The first signal $s_M(t,\theta)$ is provided by a moving probe, rotating slowly over 360 deg in a duct cross section (typically in 4 min). The angle θ is linearly related to the time t. The other microphone is in a fixed location, close to the cross section under study, and its signal $s_F(t)$ gives the phase reference (the techniques using an array of fixed microphones are discussed in another paper[20]).

Both signals s_M and s_F are digitized by an external clock triggered by a one-per-revolution pulse. The sampling frequency is a multiple of the fan rotation speed, N, chosen between 30–50 kHz. The signals are stored on a fast-acqui-

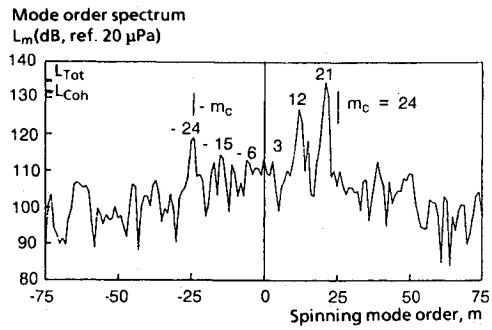

Fig. 9 Mode-order spectrum at BPF, with an upstream ring of nine rods: $B = 48$, $V = 98$, design spacing, without ICD; $N = 0.6$, $N_0 \simeq 7560$ rpm.

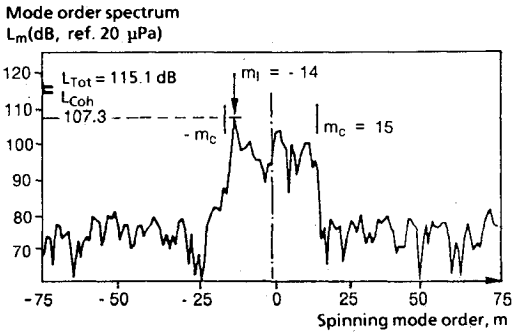

Fig. 10 Mode-order spectrum at BPF: $B = 48$, $V = 62$, maximum spacing; $N = 0.4$, $N_0 \simeq 5040$ rpm.

sition disk. The FFT S_M and S_F are computed once a second, with a resolution of 30–50 Hz. Several harmonics of N (for instance BPF and some harmonics) are then selected for the continuation of data reduction. For each one, squared amplitudes Γ_M and Γ_F of S_M and S_F and the cross-spectrum component I_{FM} are calculated as a function of t (or θ). The total level L_{Tot} of the harmonic and its coherent level L_{Coh}, i.e., the sum of the intensities of all the modes, are given respectively by

$$L_{\text{Tot}} = 10 \log (\overline{\Gamma_M})$$

$$L_{\text{Coh}} = 10 \log (\overline{|I_{FM}|^2/\Gamma_F})$$

where the upper bar denotes the average on t (or θ) during the complete scan over 360 deg. Let us remark that "*coherent*" has quite a different meaning in Secs. II and III: L_{Coh} refers to the part of the tone that is *spatially* coherent in the duct cross section, while the coherent spectra of Sec. II represent the part of the signal synchronized in *time* with the shaft rotation.

The spatial Fourier transform of the complex cross-spectrum component $I_{FM}(\theta)$ gives the mode-order spectrum $L(m)$ at the frequency under study (e.g., Figure 9). It must be emphasized that positive and negative values of m are separated, i.e., modes rotating in the same direction as the rotor and counter-rotating modes, that are generated by different loading harmonics. $L(m)$ is plotted in the range $-75 \leqslant m \leqslant +75$.

The results in the following sections are obtained with two microphones flush-mounted on the inlet duct wall at 0.60 m upstream of the rotor. It would be possible to obtain the radial profile of the acoustic field by surveys in several radial stations (e.g., Ref. 21).

B. Examples of Results in an Unlined Duct

First, let us again consider a test with the ring of 9 rods, in order to check the validity of the method. If $V = 98$, the only

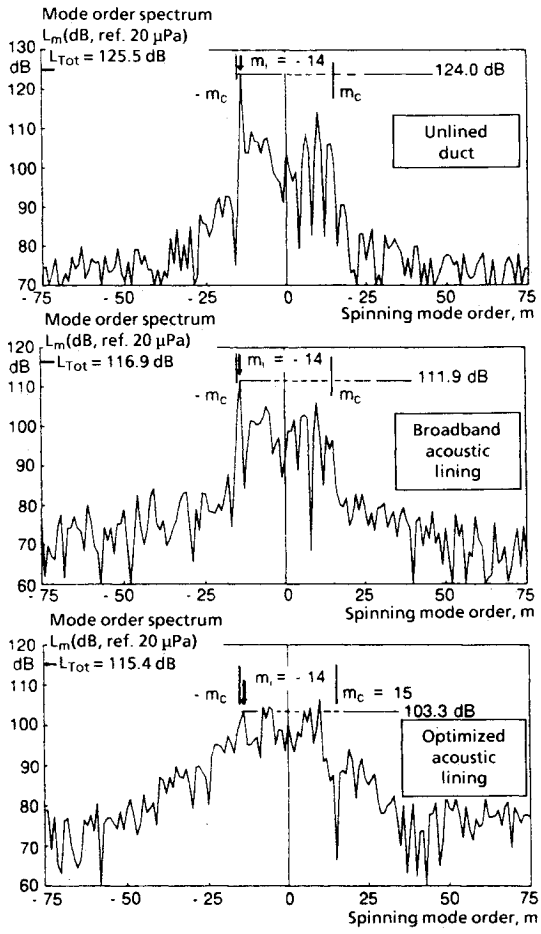

Fig. 11 Effect of acoustic linings in the inlet duct on the wave-number spectrum at BPF: $B = 48$, $V = 62$, minimum spacing; $N = 0.4$, $N_0 \simeq 5040$ rpm.

predicted propagative modes at $f_1 = BN$ are due to the interaction of the rotor with the rods: $m = B - 9j = 48 - 9j$ (j integer). Figure 9 is the modal spectrum at BPF. The value $m_c = 24$ is the last theoretical cut-on mode, taking into account the flow Mach number (also see Fig. 6c). The propagative modes $m = 21, 12, 3, \ldots$ are generated respectively by the blade loading harmonics $j = 3, 4, 5, \ldots$ due to the 9 rod wakes ($f = 9jN$). Harmonic levels tend to decrease with j (see Fig. 5b), that explains why the mode levels decrease from $m = 21$ to $m = 3$. The cutoff mode $m = -24$, due to $j = 8$, is relatively high because of its radial profile (see the following comment on Fig. 10).

Figure 10 is a result without rods and with the 62-vane stator. The first rotor-stator interaction mode propagates at BPF: $m_l = B - V = -14$. It is actually the most intense, although the rotor-OGV spacing is maximum. A cluster of several other modes, with a level well above the background data-processing noise (the ratio is about 20 dB), lie, however, within the computed range $-m_c \leqslant m \leqslant +m_c$ (with $m_c = 15$ at $N = 0.4\ N_0$). The cutoff at $m = \pm m_c$ corresponds to a sharp decrease in level. This behavior is characteristic of measurements on the wall, because values of $|m|$ close to m_c are necessarily associated with the first radial mode $\nu = 0$, and the wave radial profile is then concentrated near the wall (that is perfectly rigid in all these tests). These extraneous modes $m \neq m_l$ are due to interactions between the rotor and the inflow long-scale distortions, that generate the loading rotational harmonics of Fig. 6. The same trends have been found in similar tests of Ref. 21.

C. Efficiency of Acoustic Linings in the Inlet Duct

The previous results were obtained in an unlined duct. An important application of the spinning mode analysis is the

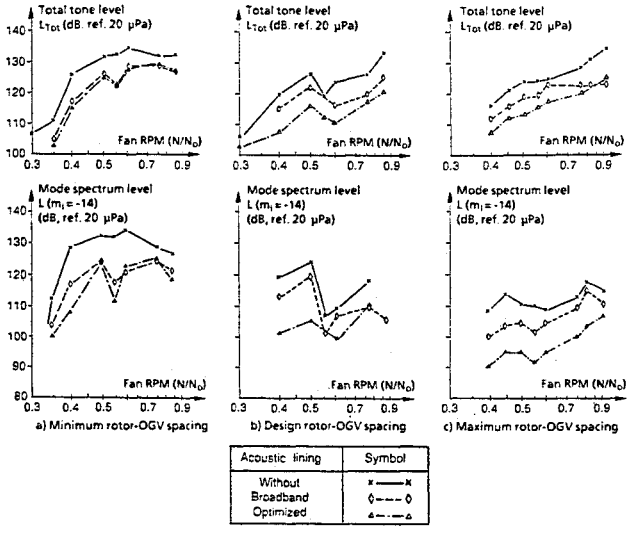

Fig. 12 Comparison of the performance of acoustic linings in the inlet duct at BPF: B = 48, and V = 62.

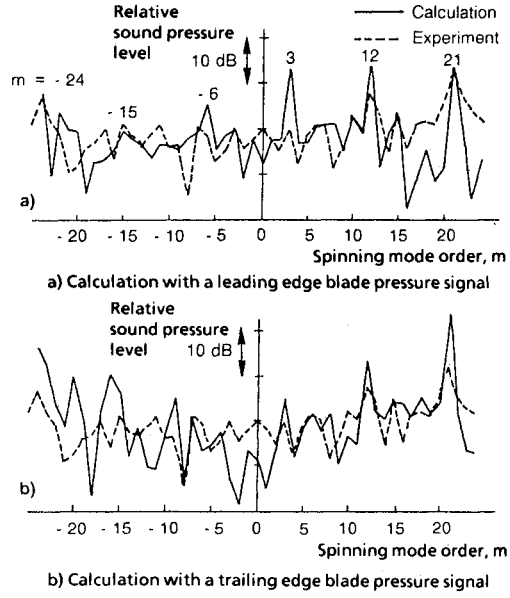

Fig. 13 Comparison of computed and measured mode-order spectra at BPF, with an upstream ring of nine rods: B = 48, V = 98, design spacing, without ICD; N = 0.6, N_0 = 7560 rpm. Prediction from a blade pressure transducer on suction side at 0.8 span.

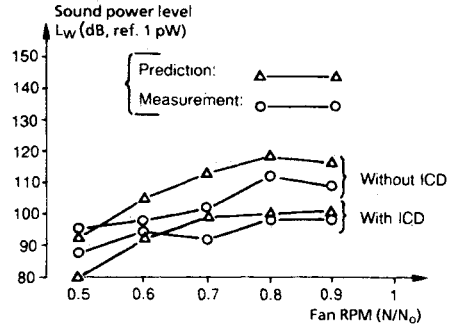

Fig. 14 Prediction of the sound-power level at BPF, from the suction side blade pressure transducer, at 0.8 span, near the leading edge, and comparison with integrated directivity measurements: B = 48, V = 98, design spacing.

characterization of acoustic linings on the inlet-duct wall. The linings used here have a length equal to the duct radius (235 mm). The measurements are made in a cross section upstream of the lining. The comparison between tests with and without lining gives an indication of the insertion loss, if it is assumed that reflections on the intake are small enough, that is nearly correct at the high frequencies under study.

Three configurations were tested, all with the 62-vane stator: 1) an unlined duct; 2) lining with resonators (honeycomb, cell depth 3 mm) covered with a wire-mesh and a perforated screen (thickness 1 mm, hole diameter 2 mm, open area ratio 0.40), designed for a broadband frequency range; and 3) lining optimized at BPF for the cuton rotor-stator interaction mode $m_l = B - V = -14$. Its acoustic impedance is optimized at $N = 0.5\,N_0$ (aircraft approach conditions, where the fan noise is dominant in the engine). The lining has the same honeycomb as above. The assembly wire-mesh/perforated screen is replaced by a single perforated plate (thickness 0.5 mm, hole diameter 1 mm, open area ratio 0.03).

The mode-order spectra at BPF are shown in Fig. 11 for the three configurations at $N = 0.4\,N_0$ and minimum rotor-OGV spacing. In the unlined duct (upper curve) the interaction mode m_l is far more intense than with maximum rotor-OGV spacing (Fig. 10, at the same speed), but all the other propagating modes have approximately the same levels (around 100 dB). The strong interaction mode is thus taken advantage of to study the acoustic linings.

Let us first compare the total BPF level L_{Tot} ($L_{\mathrm{Coh}} \simeq L_{\mathrm{Tot}}$ in the three spectra of Fig. 11). The broadband lining is a good one (insertion loss of 8.6 dB), and the optimized lining does not seem to entail a great improvement (insertion loss of 10.1 dB). However, the mode order spectra demonstrate the effectiveness of the optimized lining in attenuating the interaction mode m_l (20.7 dB instead of 12.1 dB). This effect is masked in L_{Tot} because the residual propagating modes are much less attenuated than m_l by the optimized lining, and then predominate over m_l. It is conjectured that these modes are still lower in flight than with an ICD and the insertion loss would probably be between 10–20 dB, that is an important gain over the broadband lining.

Figure 12 is a summary of these results at BPF as a function of the rotation speed, for minimum, design, and maximum rotor-OGV spacings. The upper part is the total tone level L_{Tot}, the lower part is the mode-order spectrum level at $m_l = -14$. Some runs are made at low speed, $N = 0.3\,N_0$ or $0.35\,N_0$. The levels are then very low because $m_l = -14$ is cutoff. The broadband and optimized linings are nearly equal in effectiveness at minimum spacing above $0.5\,N_0$ (Fig. 12a) because the sound levels are very high and the acoustic impedances are modified by nonlinear effects. These effects are not included in the impedance computation, so the lining is not tuned on the interaction mode in this case. The general trends at design and maximum spacings (Figs. 12b and 12c) confirm the comments on Fig. 11. The optimized lining attenuation is about 5 dB better than that of the other lining, for L_{Tot}. The difference reaches 10 dB for the isolated mode $m_l = -14$ and the corresponding insertion loss is on the order of 20 dB as compared to the rigid duct.

D. Comments on Acoustic Predictions

All the tests presented in this paper are of prime importance for research to gain a better understanding of the phenomena generating acoustic waves. They also provide input data for noise predictions. It is outside the scope of this paper to discuss theoretical noise radiation models. The methods used in our laboratories are very similar to those already published.[22] They are presented in Ref. 13. Only two examples of results are shown to illustrate the contribution of the above tests.

Figure 13 compares the mode-order spectrum measured at BPF with the upstream ring of nine rods (see Fig. 9) and those computed from two blade-pressure spectra (the experimental curves are the same in Figs. 13a and 13b). These tests with a strong interaction between the rotor blades and the wakes shed from the rods are very useful for validation purpose because some blade-loading harmonics and some spinning

modes are generated with a high level (see Figs. 5, 9, and 13).

The next step in the prediction is the summation of all the spinning modes in order to obtain the sound-power level in the duct. It is equal to the radiated sound-power level if reflections at the duct exit are neglected. This hypothesis seems to be valid at high frequency (such as BPF). Figure 14 is a plot of BPF sound power levels vs the rotation speed, with and without the inflow control device (without the rods). Experimental data are obtained by integrating the directivity patterns measured in the upstream anechoic chamber. Predicted values are deduced from blade-pressure spectra (OGV pressure fluctuations are not taken into account because they are expected to produce a negligible contribution to upstream radiated noise, as has been pointed out in the comment on Fig. 4). Figure 14 shows that there are some discrepancies between predicted and measured absolute sound-power levels. They are probably due to a crude simplification in the computations, assuming a compact point source at the blade transducer location. However, the differences between sound-power levels with and without ICD agree with the experimental results.

Conclusion

The usual acoustic tests of turbofan engines are often limited to far-field directivity surveys. This is insufficient for accurate knowledge of the sources, that is needed for predicting and reducing the radiated noise. The aerodynamic computations are also still unable to calculate the actual noise sources.

Some special experiments have been developed, with blade- and vane-pressure transducers, and spinning-mode analysis in the inlet duct. Several examples of applications are discussed. It is shown that an inflow-control device reduces the aerodynamic disturbances by about 10 dB, as expected. Even with such a device, it is difficult to measure the attenuation of a duct lining that would be produced in flight in a static bench, because of the residual inflow distortion noise. The rotor-stator interaction tones are isolated by the modal analysis, and it is then found that a lining with a length of one duct radius, optimized for the blade-passing frequency, could give an insertion loss up to 20 dB on the rotor-stator interaction mode.

Finally, a few comparisons with prediction programs assess the validity of such experimental work. The implementations of blade- and vane-pressure transducers and of spinning-mode analysis technique are long and expensive, but there is no other alternative to further the understanding of fan or compressor noise. Some tests in special facilities with anechoic rooms could also be avoided in the future, since these results show that good acoustic characterizations may be deduced from internal measurements in the fan.

Acknowledgments

This work is supported by the Service Technique des Programmes Aéronautiques and the Direction Générale de l'Aviation Civile. Several teams are involved in the pressure transducer experiments: they are designed, manufactured and fitted by the ONERA Electronics Division; the electronics is assumed by ELECMA, a SNECMA Division. The tests are made possible thanks to all the staff of the 5C2 facility.

References

[1]Morfey, C. L., "The Acoustics of Axial Flow Machines," *Journal of Sound and Vibration*, Vol. 22, No. 4, 1972, pp. 445–466.

[2]Tyler, J. M., and Sofrin, T. G., "Axial Flow Compressor Noise Studies," *Society of Automotive Engineers Transactions*, Vol. 70, 1962, pp. 309–332.

[3]Lévy, S., Lambourion, J., Malarmey, C., Pérulli, M., and Rafine, B., "Direct Experimental Verification of the Theoretical Model Predicting Rotor Noise Generation," AIAA Paper 79-0658, March 1979.

[4]Fourmaux, A., "Computation of Unsteady Flows in Turbomachine Cascades," *Proceedings of the 15th Congress of the ICAS*, Vol. 2, London, Sept., 1986, pp. 951–956.

[5]Heller, H. H., and Widnall, S. E., "The Role of Fluctuating Forces in the Generation of Compressor Noise," NASA CR-2012, May 1972.

[6]Hanson, D. B., "Spectrum of Rotor Noise Caused by Atmospheric Turbulence," *Journal of the Acoustical Society of America*, Vol. 56, No. 1, 1974, pp. 110–126.

[7]Hanson, D. B., "A Study of Subsonic Fan Noise Sources," AIAA Paper 75-468, March 1975.

[8]Mugridge, B. D., "The Measurement of Spinning Acoustic Modes Generated in an Axial Flow Fan," *Journal of Sound and Vibration*, Vol. 10, No. 2, 1969, pp. 227–246.

[9]Bolleter, U., and Crocker, M. J., "Theory and Measurement of Modal Spectra in Hardwalled Cylindrical Ducts," *Journal of the Acoustical Society of America*, Vol. 51, No. 5, Pt. 1, 1972, pp. 1439-1447.

[10]Harel, P., and Pérulli, M., "Measurement, in a Duct, of the Space-Structure of the Discrete Frequency Noise Generated by an Axial Compressor," *Journal of Sound and Vibration*, Vol. 23, No. 4, 1972, pp.487–506.

[11]Ho, P. Y., Smith, E.B., and Kantola, R. A., "An Inflow Turbulence Reduction Structure for Scale Model Fan Testing," AIAA Paper 79-0655, March 1979.

[12]"Methods of Controlling Distortion of Inlet Airflow during Static Acoustical Tests of Turbofan Engines and Fan Rigs," Society of Automotive Engineers, Inc., Aerospace Information Rept. AIR 1935, Warrendale, PA, Feb. 1985.

[13]Raffy, P., Lévy, S., Lambourion, J., and Chatanier, M., "Investigation of Subsonic Fan Noise Sources by Fluctuating Pressure Measurements on Rotating Blades," AIAA Paper 77-1321, Oct. 1977; see also *AIAA Journal*, Vol. 16, No. 8, 1978, pp. 777–778.

[14]Franke, G. F., and Henderson, R. E., "Unsteady Stator Response to Upstream Rotor Wakes," AIAA Paper 79-0579, March 1979; see also *Journal of Aircraft*, Vol. 17, No. 7, 1980, pp. 500–507.

[15]Preisser, J. S., Schoenster, J. A., Golub, R. A., and Horne, C., "Turbofan Engine Blade Pressure and Acoustic Radiation at Simulated Forward Speed," AIAA Paper 81-0096, Jan. 1981; see also *Journal of Aircraft*, Vol. 20, No. 4, 1983, pp. 289–297.

[16]Schoenster, J. A., "Fluctuating Pressure Measurements on the Fan Blades of a Turbofan Engine During Ground and Flight Tests," AIAA Paper 83-0679, April 1983.

[17]Kraft, R. E., Paas, J. E., and Clark, L. R., "Effects of Multi-Element Acoustic Treatment on Compressor Inlet Noise," AIAA Paper 76-515, July 1976.

[18]Posey, J. W., "Comparison of Cross-Spectral and Signal Enhancement Methods for Mapping Steady-State Acoustic Fields in Turbomachinery Ducts," NASA TM-X-73916, Aug. 1976.

[19]Lévy, S., Canard, S., and Kerviel, P., "Study of Propagating Acoustic Sources in a Fan Intake by Modal Analysis of Tone Noise," *Proceedings of Inter-noise 88*, Vol. 2, Avignon, France, Aug.–Sept., 1988, pp. 751–754.

[20]Blacodon, D., and Lévy, S., "Space-Structure Determination of the Acoustic Field Generated by a Helicopter Turboshaft Engine," AIAA Paper 90-4012, Oct. 1990.

[21]Zandbergen, T., "Experimental Investigation of Rotor Wake/Stator Interaction Noise Generation by Acoustic Mode Measurements," AIAA Paper 89-1126, April 1989.

[22]Mani, R., "Isolated Rotor Noise Due to Inlet Distortion or Turbulence," NASA CR-2479, Oct. 1974.

[23]Nakamura, Y., and Isomura, K., "Detection of Fan Acoustic Mode," AIAA Paper 87-2700, Oct. 1987.